

# Evaluating earthquake-related ground failure mapping by combined traditional and modern methods

Takayuki NAKANO<sup>a, \*</sup>, Hiroshi UNE<sup>a, +</sup>, Kazuki YOSHIDA<sup>a</sup>, Satoshi FUJIWARA<sup>a</sup>, Tomokazu KOBAYASHI<sup>a</sup>

<sup>a</sup> Geospatial Information Authority of Japan, [nakano-t96fj@mlit.go.jp](mailto:nakano-t96fj@mlit.go.jp), [hiroune@mb.infoweb.ne.jp](mailto:hiroune@mb.infoweb.ne.jp), [yoshida-k96g4@mlit.go.jp](mailto:yoshida-k96g4@mlit.go.jp), [fujiwara-s2vq@mlit.go.jp](mailto:fujiwara-s2vq@mlit.go.jp), [kobayashi-t96dv@mlit.go.jp](mailto:kobayashi-t96dv@mlit.go.jp)

\* Corresponding author

+ Former affiliation

**Abstract:** A wide range of ground failure such as earthquake faulting (surface rupture), landslides, and liquefaction occur after a large earthquake. In this study, in order to rapidly determine the distribution of failure over a wide area after an earthquake, we combined traditional methods such as aerial photo interpretation and modern methods such as unmanned aerial vehicle (UAV) or interferometric synthetic aperture radar (InSAR) techniques. Moreover, elevation variations obtained using DEMs and the structure from motion and multi-view stereo (SfM-MVS) technique were employed to understand local ground deformation factors, such as reclaimed valley deformation. Using ortho-mosaic images, surface fissures caused by the 2016 Kumamoto Earthquake in Japan were rapidly interpreted and mapped, which enabled early interpretation of the ground failure situation. Furthermore, surface displacement properties extracted from SAR interferograms allowed for more advanced earthquake fault detection; surface displacement associated with liquefaction was also identified from SAR interferograms. In addition, InSAR was used to detect reclaimed valley deformation. Comparing this with the reclaimed valley distribution map created by the SfM-MVS technique improved our understanding of this phenomenon. However, many of these techniques require large amounts of manpower and time and can be influenced by differences in analyst skill level. In future, the development of mechanically automated ground failure identification will improve earthquake disaster responses.

**Keywords:** 2016 Kumamoto Earthquake, ground failure, ortho-mosaic image interpretation, InSAR, SfM-MVS

## 1. Introduction

After a large earthquake, various types of ground failure may occur, such as earthquake faulting (surface rupture), landslides, and liquefaction. For an effective disaster response, it is important that governments can rapidly detect the distribution of ground failure over a wide area.

Interpretation using aerial photos and satellite images is an effective, traditional method for ground failure mapping. Although conventional aerial photos are taken by aircraft, the use of unmanned aerial vehicles (UAV) has also progressed recently, which is suitable for high-resolution video and images over a small area.

Interferometric Synthetic Aperture Radar (InSAR) technology, which is mainly aimed at detecting crustal deformation associated with earthquakes, utilizes SAR images from two different periods captured in the same location (Hanssen, 2001). It is an innovative approach that is also effective for identification of surface displacement such as secondary fault displacement and minor slope deformation induced by earthquakes (Une et al., 2008; Fujiwara et al., 2016; Nakano et al., 2016b etc.). Furthermore, earthquakes can induce landslide-like deformation in artificially filled-up (reclaimed) valley; it

is possible that this type of deformation can be detected by InSAR, which detects slight slope deformations of landslides. In order to determine the factors affecting local surface displacement in reclaimed land, it is necessary to understand the historical background of the topography. Although the amount of topographic variation can be detected by the difference between a previous digital elevation model (DEM) and the current DEM, previous DEMs cannot be easily acquired. Thus, SfM multi-view stereo photogrammetry (SfM-MVS) can be used instead, which has shown remarkable advances in recent years. SfM-MVS can automatically restore the captured position of each photograph and the three-dimensional shape of the object using multiple images from a large number of viewpoints. Furthermore, it can generate a detailed three-dimensional model of the object (e.g. Furukawa and Ponce, 2010; Mitsugami, 2011). Additionally, by using the SfM-MVS technique to create a digital surface model (DSM) from past aerial photographs and filtering it as a pseudo DEM, the amount of topographic variation can be easily obtained (Nakano, 2017).

In this study, we focus on surface fissures, soil liquefaction and associated surface displacement, and

reclaimed valley deformation related to earthquakes and map the relevant ground failure using a combination of traditional methods; i.e., aerial photo (ortho-mosaic image) interpretation and modern methods; i.e., UAV video, InSAR technology, and SfM-MVS technique. We then discuss the applicability and challenges of these combined techniques.

## 2. Mapping Outline

### 2.1 Targets

We map the following types of ground failure caused by the 2016 Kumamoto Earthquake (April 16, 2016, Mj 7.3) in Japan: 1) general surface fissures including surface earthquake faults (surface rupture) and cracks due to seismic motion or gravitational deformation; 2) soil liquefaction (sand volcano) traces and related surface displacement; and 3) reclaimed valley deformation.

### 2.2 Mapping Methods

#### 2.2.1 Surface fissures

For type 1 ground failure, traditional ortho-mosaic image interpretation was performed. If the ortho-mosaic image was hard to interpret, additional confirmation was performed using a single image with higher resolution. The fissures were mapped directly on GIS from ortho-mosaic images imported into GIS. Misreading was reduced by having multiple people perform the interpretation. Surface fissures caused by the earthquake were acquired by comprehensively mapping linear deviations in continuous features and differences in shading. If a feature was not easily identified as belonging to this earthquake, aerial photos taken before the earthquake were also utilized. However, there was a slight discrepancy in the acquisition criteria due to differences in analyst skill levels.

Regarding more modern methods, surface earthquake faults in a local area were interpreted from UAV videos and linear surface displacements were extracted from SAR interferograms. In a part of the areas where surface earthquake fault mapping could not be identified sufficiently by aerial photo interpretation, identification of the lateral shift direction and accompanying en échelon structure was performed using low-flying UAV video. The SAR interferogram technique is described in detail in Fujiwara et al. (2016). Here, linear phase discontinuities indicating linear surface displacements were extracted from SAR interferograms. A field survey was also conducted to verify surface fissures.

#### 2.2.2 Liquefaction (sand volcano) traces and associated surface displacement

For type 2 ground failure, traditional ortho-mosaic image interpretation and GIS mapping were performed, which involved interpreting traces of sand volcanoes and wet parts caused by the eruption of groundwater. Small-scale and large-scale liquefaction information was acquired using point data and polygon data, respectively.

Regarding more modern methods, liquefied areas and surface displacement areas due to liquefaction were extracted from SAR interferograms. It is noted that interference (coherence) decreases in a liquefied area (Kobayashi et al., 2011; Ishitsuka et al., 2012) and the interferogram becomes noise-like. Even in the Kumamoto Earthquake, similar feature regions were identified in the SAR interferograms. In addition, the phase change region considered as lateral movement of the ground due to liquefaction was extracted, and the actual deformation was confirmed through a field survey.

#### 2.2.3 Reclaimed valley deformation

In the 2016 Kumamoto Earthquake, several areas of reclaimed valley suffered from landslide-like damage. Phase changes such as noise spots appeared in the SAR interferogram at these sites due to large changes in the ground surface. By extracting these phase changes and conducting a field survey, we confirmed that the actual deformation and phase changes were consistent.

To determine the extent of reclaimed valley, a DSM of that time was created using aerial photos prior to construction using the SfM-MVS technique. The DSM was then converted to a pseudo DEM by filtering to obtain the lowest value within a certain range (Nakano, 2017). Then, a reclaimed valley distribution map was created by taking the difference between the pre-construction and post-construction DEMs. We then compared the reclaimed valley distribution map with the phase change region in the SAR interferogram to examine the relationship between the two.

## 2.3 Data

### 2.3.1 Aerial photos (ortho-mosaic image)

The aerial photos used to interpret each type of ground failure were taken by the Geospatial Information Authority (GSI) of Japan on the 16<sup>th</sup>, 19<sup>th</sup>, 20<sup>th</sup>, and 29<sup>th</sup> April 2016, after the earthquake. The ground sampling distance (GSD) of the aerial photo was approximately 20 cm. Although ortho-mosaic images were created from the aerial photos, it has been resampled and the GSD is greater than 20 cm. The spatial coverage of ortho-mosaic images is shown in Figure 1. Type 1 and 2 ground failure were interpreted and mapped within these areas respectively.

### 2.3.2 UAV video

The UAV video data used in this research covered the surface earthquake fault in Minamiaso Village on the west side of Mt. Aso and was obtained from the GSI of Japan. This video was a 4K video shot with a DJI Phantom 3 and is available at: (<https://www.youtube.com/watch?v=bS6ftodIHeI&feature=youtu.be>). The characteristics of surface earthquake faults were interpreted from this video and captured images.

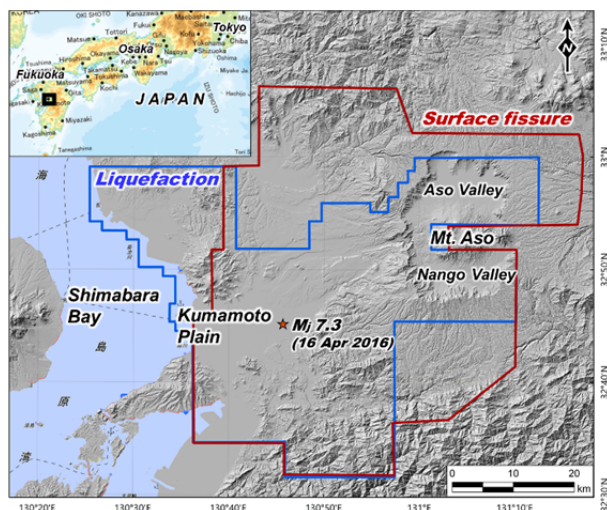


Figure 1. Coverage of ortho-mosaic images. Brown frame: interpretation range of surface fissures, blue frame: interpretation range of liquefaction.

### 2.3.3 SAR interferogram

SAR interferograms were used to extract type 1 and type 3 ground failure. The SAR interferograms were analyzed by the GSI of Japan using data of the Earth Observation Satellite “ALOS-2” launched by JAXA. We predominantly used interferograms generated by March 7, 2016 and April 18, 2016 and April 15, 2016 and April 29 image pairs.

### 2.3.4 SfM-MVS analysis

The SfM-MVS technique was used for data acquisition of reclaimed valley to enhance our understanding of type 3 ground failure in combination with InSAR technology. Pre-construction aerial photographs used for SfM-MVS processing were monochrome aerial photos of 1/20,000 scale taken by the GSI of Japan in the 1960s. A 5-m grid DEM acquired by airborne laser scanning in 2009 was used for the post-construction DEM.

## 3. Mapping Results

### 3.1 Surface fissures

Figure 2(a) shows the distribution of surface fissures associated with the 2016 Kumamoto Earthquake, which were extracted by the traditional method of ortho-mosaic image interpretation. They are distributed linearly along known active faults (black lines in Figure 2(a)). Most of the surface earthquake faults (Kumahara et al., 2016; blue lines in Figure 2(a)) confirmed in the field survey were extracted, except for those in the mountains. In addition, a linear fissure group crosses the Kumamoto plain (A in Figure 2(a)) from downtown Mashiki Town, where extreme damage occurred. Although active underground faults have been reported here (Yoshimi et al., 2018), no fault displacement topography was observed on the ground. Furthermore, fissures associated with liquefaction or large lateral movement of the ground mass (Nakano et al., 2016a; Tsuji et al., 2017; Fujiwara et al., 2017 etc.) were also extracted locally in Aso Valley.

The interpreted surface fissures are divided into three types according to their formation mechanism: fissures due to surface earthquake faulting, fissures associated with liquefaction, and fissures caused by gravitational deformation. Among these, examples of surface earthquake faults interpreted from aerial photos and UAV videos are shown below.

In the ortho-mosaic image, fissures with linear or en échelon continuity and notable lateral displacement are considered to be due to surface earthquake faulting (e.g. Figure 3). In Mitake district, Mashiki Town, right lateral slip of approximately 0.7 m was confirmed by the field survey (Figure 3).

Figure 4 compares aerial images with those captured from the UAV video of surface earthquake faults in Kawayo district, Minamiaso Village. The blurred surface earthquake faults in the aerial photo can be clearly identified by their en échelon structure in the UAV image. Figure 2(b) shows the linear surface displacements derived from the SAR interferograms (Fujiwara et al., 2016). Figure 2(c) shows the surface fissures of Figure 2(a) superposed with the linear surface displacements of Figure 2(b). This reveals that the SAR interferogram can extract even minor surface displacements and those in the mountainous area under the forest (Figure 5), which cannot be extracted by ortho-mosaic image interpretation. As described above, surface fissure distribution mapping is useful for detecting the distribution of ground failure over a wide area. However, interpretation using only conventional aerial photo (ortho-mosaic image) is limited, and is more effective when UAV video and SAR interferograms are combined.

### 3.2 Liquefaction (sand volcano) traces and associated surface displacements

Figure 6 shows the distribution of liquefied areas (sand volcanoes) associated with the 2016 Kumamoto Earthquake, extracted by ortho-mosaic image interpretation. Liquefaction was intensive in the Kumamoto plain, Aso Valley, and Nango Valley. Normal sand volcanoes have a white to brown color under dry conditions (Figure 7(a)), but dark gray color spots appear in Aso Valley due to the eruption of black scoria and a high ground water level (Fig. 7(b)). Although field confirmation of liquefaction sites is rarely conducted, we observed no significant differences from the liquefaction distribution map produced by Wakamatsu et al. (2017), which was based on similar aerial photo interpretation and field survey.

As described above, in the liquefied area, the coherence of SAR interferograms decreases and appears as a noise-like phase change. Figure 8 shows the example of the Kumamoto earthquake. In the Kumamoto city area, we observed a belt-shaped noise-like phase change meandering in the north-south direction. In this area, liquefaction damage was also confirmed by ortho-mosaic image interpretation and the field survey (Wakamatsu et al., 2017 etc.); thus, we presume that coherence of the SAR interferograms was reduced by the sand volcanoes.

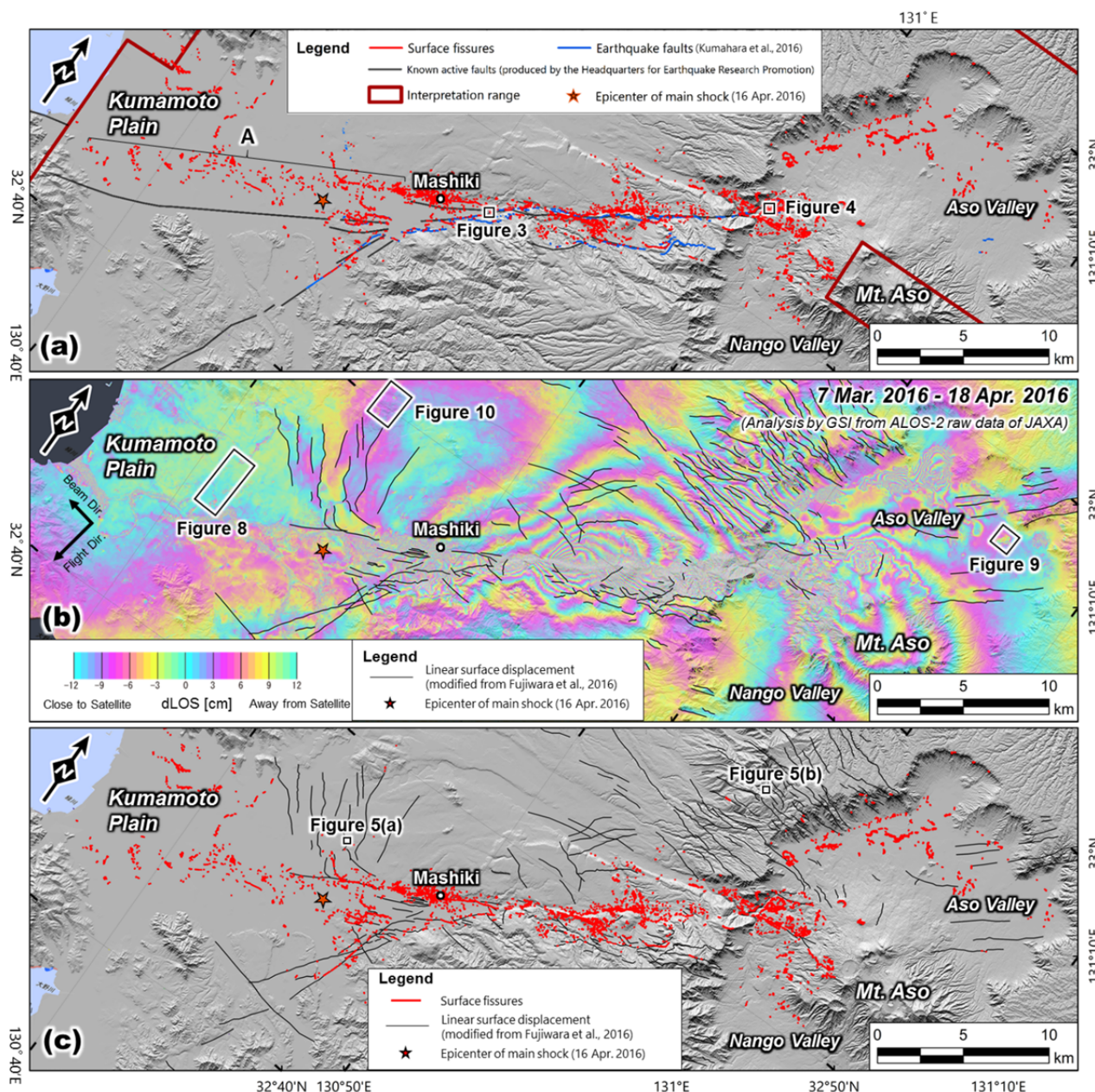


Figure 2. (a) Surface fissure distribution map for the 2016 Kumamoto Earthquake interpreted from ortho-mosaic images. (b) SAR interferogram showing linear surface displacements (modified from Fujiwara et al., 2016). (c) The surface fissures of Figure 2(a) superposed with the linear surface displacements of Figure 2(b).

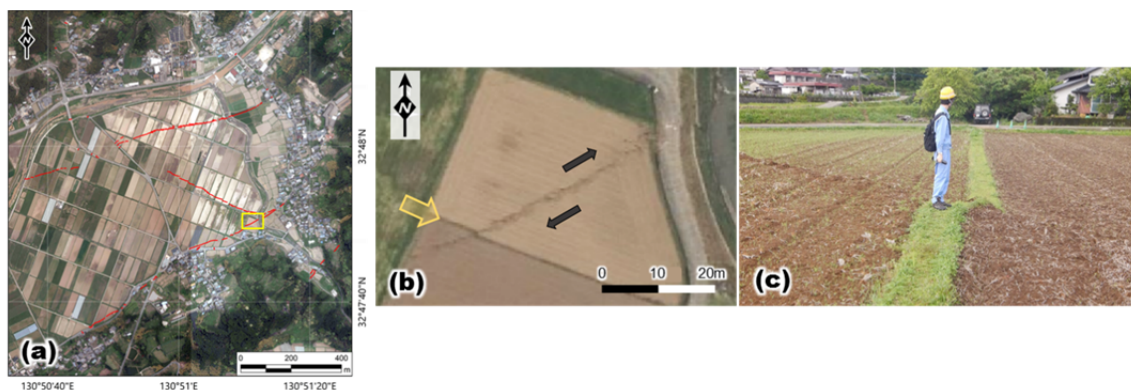


Figure 3. An example surface earthquake fault that appeared in Mitake district, Mashiki Town (location shown in Figure 2(a)). (a) Red lines show the trace of the surface earthquake fault (the background is an ortho-mosaic image taken on April 16, 2016). (b) Enlarged image (single image) within the yellow frame of (a). (c) Ground photo taken at the yellow arrow location in (b).



Figure 4. UAV video image of surface earthquake faults that appeared in Kawayo district, Minamiaso Village (upper figure) and aerial photograph (single image) of the same area (lower figure).



Figure 5. (a) Slight surface crack (shown by white arrows) that appeared in Kengun district, Kumamoto City (location shown in Figure 2(c)). (b) Surface earthquake fault (shown by white arrows) confirmed in the mountains in the northwest part of the outer rim of the Aso caldera (location shown in Figure 2(c)).

Unlike the decrease of coherence associated with sand volcanoes, the ground mass can also move laterally due to liquefaction without much change in the condition of the ground surface. An example of this was observed in Aso Valley induced by the Kumamoto Earthquake (Figure 9). Although it is difficult to quantify the amount and direction of displacement from the SAR interferogram, the field survey revealed clear surface displacements with opening and shortening cracks in this area (Figure 9).

As described above, the distribution of liquefaction (sand volcanoes) can essentially be extracted by ortho-mosaic image interpretation, but InSAR technology enables additional screening of the interpretation area of the ortho-mosaic image, revealing lateral movement where no sand volcanoes appear on the ground surface.

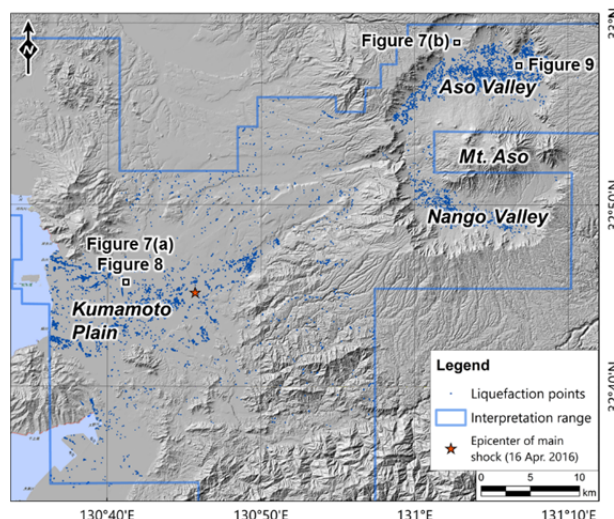


Figure 6. Distribution map of liquefied areas (sand volcanoes) associated with the 2016 Kumamoto Earthquake extracted by ortho-mosaic image interpretation.

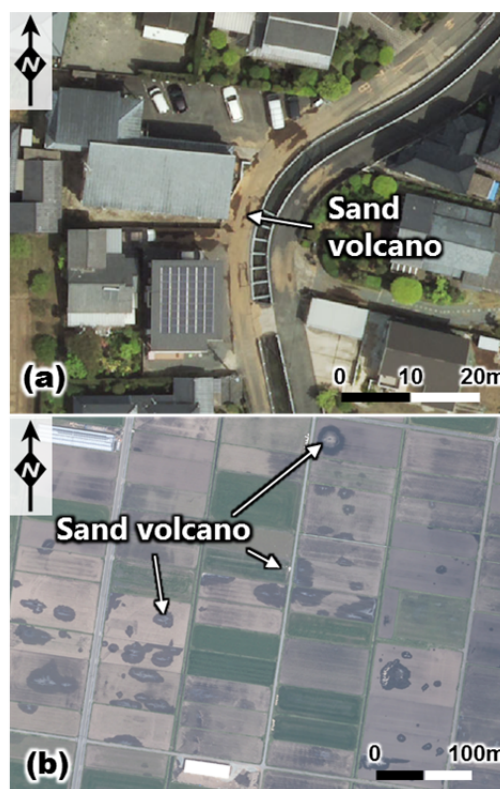


Figure 7. (a) Normal sand volcanoes in Kumamoto city area (location shown in Figure 6), and (b) dark gray sand volcanoes in Aso Valley (location shown in Figure 6).

### 3.3 Reclaimed valley deformation

Extraction of reclaimed valley deformation was achieved using only InSAR. For the Kumamoto Earthquake, after deformation of the reclaimed valley was confirmed locally, aerial photo interpretation was performed again, but associated cracking of the ground surface was rarely identified.

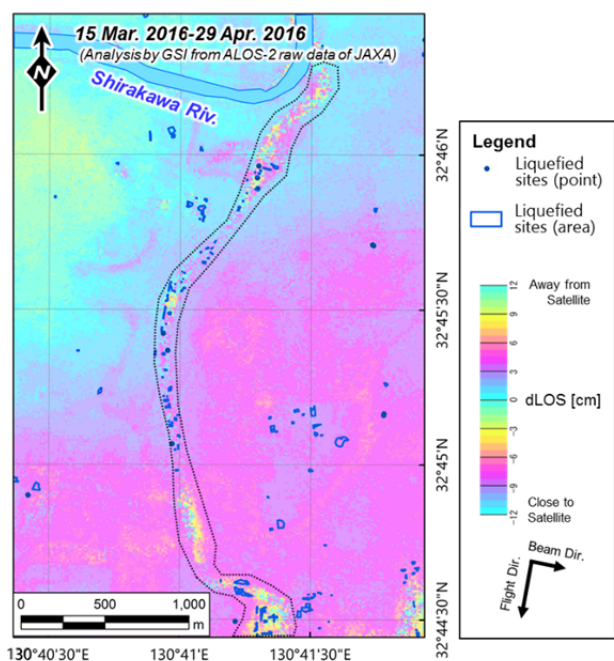


Figure 8. Noise-like phase change (region surrounded by black dotted lines) associated with liquefaction (sand volcanoes) in Kumamoto city area and distribution of liquefaction interpreted from aerial photos.

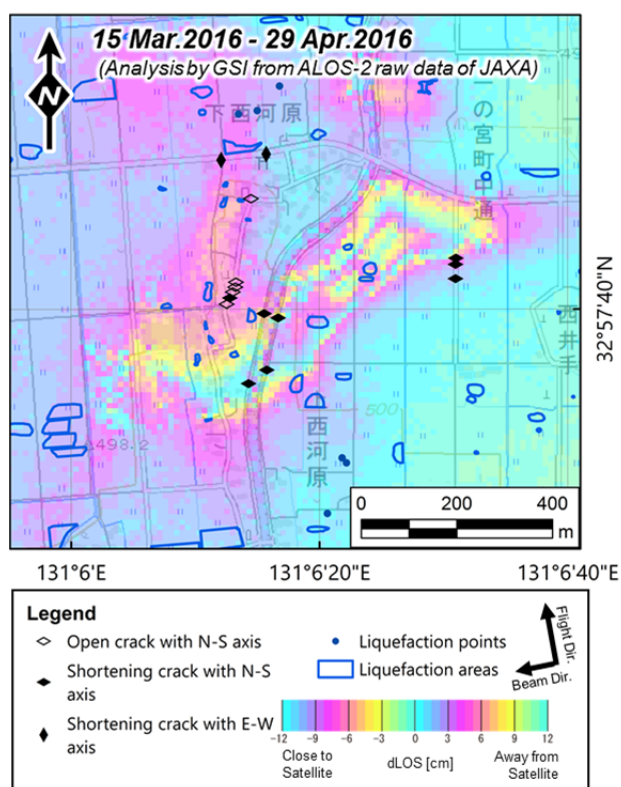


Figure 9. Phase change of lateral movement of ground surface associated with liquefaction on the SAR interferogram at Aso Valley (position shown in Figure 6), liquefaction sites distribution and surface displacements identified by field survey.

Figure 10(a) shows an example of a phase change indicating deformation of reclaimed valley. As described above, these phase changes have the appearance of noise-like spots, but the amount of deformation cannot be

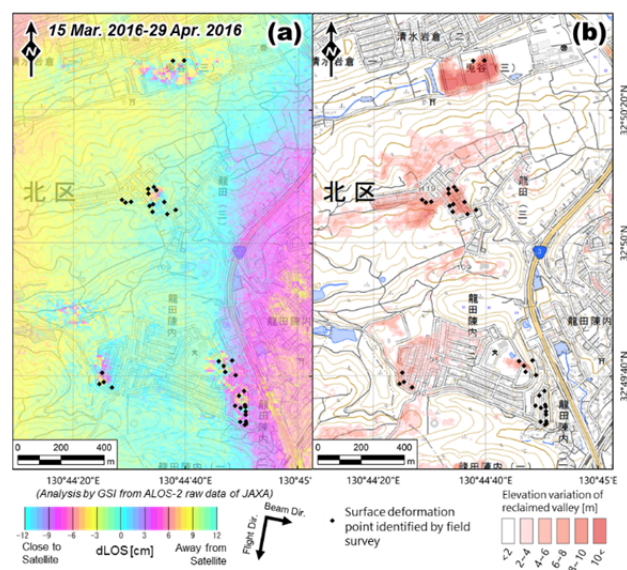


Figure 10. (a) An Example of phase change of reclaimed valley deformation on SAR interferogram, (b) reclaimed valley distribution map created by using SfM-MVS technique. Black diamond marks in both figures show the position of surface deformation found out by field survey.

identified. However, the area of deformation is largely identifiable. As a result of site investigations, deformation (e.g. surface cracks) of surface structures (roads, building foundations, retaining walls) was observed in the phase change area (black diamond marks in Figure 10).

Figure 10(b) shows the reclaimed valley distribution map created by the difference between the pseudo DEM generated from aerial photos using the SfM-MVS technique and the post-construction DEM of the same area as Figure 10(a). The deformation area detected by InSAR almost coincides with the area of reclaimed valley. Thus, deformation of reclaimed valley, which is difficult to identify in aerial photographs (ortho-mosaic images) can be extracted using InSAR. It is possible that InSAR can also be used to extract deformed reclaimed valley over broader earthquake disaster areas.

## 4. Discussion: Applicability and challenges

### 4.1 Interpretation of surface fissures

Earthquake surface fissure mapping can be conducted using the traditional method of interpreting aerial photos (ortho-mosaic images), which can detect ground failure over a wide area if conducted soon after the photos are taken. It is also useful for disaster response and recovery planning. In fact, the results of surface fissure mapping were used in the disaster response by the local disaster countermeasure headquarters and in subsequent research, as well as wider research on earthquake mechanisms and local surface displacement (Goto et al., 2017; Fujiwara et al., 2017, etc.) and active fault map production (Suzuki et al., 2017; Kumahara et al., 2017). In addition, the identified linear fissure group crossing the Kumamoto plain (A in Figure 2(a)) may have an influence on underground fault motion, which is a new finding. Furthermore, by combining this method with more

modern methods such as InSAR and UAV, we can detect surface displacements and characteristics that cannot be identified by aerial photo interpretation alone.

On the other hand, if ground failure occurs over a wide area, as in the Kumamoto Earthquake, interpretation of ortho-mosaic images requires considerable manpower and time. In the case of the Kumamoto Earthquake, every time an aerial photo was taken, it was interpreted by several different people. It took four days to publish the first surface fissure distribution map online and provide it to related organizations after the aerial photography; however, it then took almost a month to complete the interpretation due to other disaster response duties. Also, as mentioned above, although the interpretation criteria are provided, individual differences exist in the interpretation result, and the standards are not sufficiently unified.

Extraction of linear phase discontinuities from SAR interferograms has strong research applications, yet one analyst took more than a month to complete the interpretation for this earthquake. Thus, this method has similar issues to ortho-mosaic images.

Considering the above, it is necessary to clarify the interpretation criteria and improve analyst skill levels when using the traditional method. If emphasis is placed on fewer analysts and reduced workloads in future, it is expected that surface fissure extraction will become automated through, for example, deep learning.

#### **4.2 Interpretation of liquefaction (sand volcano) traces and associated surface displacements**

It is possible to almost fully interpret the liquefied area (sand volcano) by aerial photos (ortho-mosaic image), yet combining this with InSAR enables screening of the interpretation area of the ortho-mosaic image and extraction of lateral ground movement. Liquefaction leads to building tilting, road deformation, underground infrastructure damage, etc., and the influence on human life is significant. Therefore, it is important to detect the distribution of liquefaction in disaster recovery planning and cause investigation.

However, as for surface fissures, high manpower and time costs are required for interpretation of ortho-mosaic image, and sometimes cases are difficult to identify. In the case of the Kumamoto Earthquake, it took two analysts several months to perform the interpretation of ortho-mosaic image. Therefore, we expect that automated technology will also be developed for extraction of liquefaction trace.

#### **4.3 Identification of reclaimed valley deformation**

Seismic deformation of reclaimed valley has occurred in previous earthquakes; for example, the 2011 Tohoku Earthquake off the Pacific coast in Japan. However, deformation was not detected by InSAR at the time of the Tohoku Earthquake, presumably because the resolution of the SAR satellite (ALOS) at that time was not sufficient. In other words, the Kumamoto Earthquake is the first example of reclaimed valley deformation

detection. Extraction of the reclaimed valley deformation area by this method is useful for early detection of the damage distribution in large-scale disasters. However, as described above, the deformation has the appearance of a noise-like spot and is difficult to distinguish from other noise. Therefore, its application is limited to cases where the peripheral coherence is high. Moreover, certain expertise is required for the interpretation. Automated extraction is also expected for this type of deformation, but it is currently difficult to use deep learning due to the small number of real-world examples.

Determining reclaimed valley distribution is important to help understand the mechanism of reclaimed valley deformation. Conventionally, it involved considerable labor, yet using the SfM-MVS technique has made it relatively easy. However, it involves creating a DSM using SfM-MVS, and the subsequent pseudo DEM created exhibits considerable error, especially in forest areas. Therefore, as the reclaimed valley distribution map also has considerable error, care should be taken when applying this map. Nonetheless, it is sufficient for providing an early interpretation during disaster response, and the reclaimed valley distribution map by this method was used for actual disaster response work in the event of the 2018 Hokkaido Eastern Iwate Earthquake in Japan.

### **5. Conclusions**

This study evaluates the capabilities of both traditional and modern methods for large-scale, rapid mapping of multiple types of ground failure associated with earthquakes. The traditional method was ortho-mosaic image interpretation and the modern methods included UAV video, InSAR technology, and the SfM-MVS technique. The surface fissure distribution map for the Kumamoto Earthquake was useful for early detection of general ground failure and disaster research. Also, surface displacement characteristics extracted from SAR interferograms enhanced our understanding of the earthquake faults. The surface displacement associated with liquefaction was also effectively identified from SAR interferograms. In addition, InSAR detected reclaimed valley deformation; comparing it with the reclaimed valley distribution map created using SfM-MVS provided additional information of this phenomenon. However, the majority of these methods require expertise and large amounts of manpower and time, and can be influenced by individual differences in the skill levels of analysts. In the future, mechanical automation of ground failure identification will be key to ensure a more effective disaster response.

### **6. Acknowledgements**

ALOS-2 data were provided by the Earthquake Working Group under a cooperative research contract with JAXA. The ALOS-2 data belong to JAXA.

### **7. References**

Fujiwara, S., Morishita, Y., Nakano T., Kobayashi, T. and Yurai, H. (2017). Non-tectonic liquefaction-induced

- large surface displacements in the Aso Valley, Japan, caused by the 2016 Kumamoto earthquake, revealed by ALOS-2 SAR, *Earth and Planetary Science Letters*, 474, 457-465, DOI: 10.1016/j.epsl.2017.07.001
- Fujiwara, S., Yurai, H., Kobayashi, T., Morishita, Y., Nakano, T., Miyahara, B., Nakai, H., Miura, Y., Ueshiba, H., Kakiage Y. and Une, H. (2016). Small-displacement linear surface ruptures of the 2016 Kumamoto earthquake sequence detected by ALOS-2 SAR interferometry, *Earth, Planets and Space*, 68:160, DOI: 10.1186/s40623-016-0534-x
- Furukawa, Y. and Ponce, J. (2010). Accurate, dense, and robust multiview stereopsis: *IEEE Transactions on Pattern Analysis and Machine Intelligence*, 32, 1362-1376, DOI:10.1109/TPAMI.2009.161
- Goto, H., Tsutsumi, H., Toda, S. and Kumahara, Y. (2017): Geomorphic features of surface ruptures associated with the 2016 Kumamoto earthquake in and around the downtown of Kumamoto City, and implications on triggered slip along active faults. *Earth, Planets and Space*, 69:26. DOI:10.1186/s40623-017-0603-9
- Hanssen, R. (2001). *Radar interferometry: data interpretation and error analysis*, Kluwer.
- Ishitsuka, K., Tsuji, T., Matsuoka, T. and Mizuno, T. (2012). Surface displacement induced by liquefaction of the 2011 Tohoku-oki Earthquake in Tokyo Bay area using InSAR analysis, *Journal of Japan Society of Civil Engineers, Ser. C (Geosphere Engineering)*, 68(1), 175-182. (in Japanese with English abstract)
- Kobayashi, T., Tobita, M., Koarai, M., Otoi, K. and Nakano, T. (2011). Liquefaction area associated with the 2011 off the Pacific coast of Tohoku Earthquake, inferred from interferometric SAR coherence change, *Journal of GSI of Japan*, 122, 143-151 (in Japanese).
- Kumahara, Y., Okada, S., Kagohara, K., Kaneda, H., Goto, H. and Tsutsumi, H. (2017): 1:25,000 Active Fault Map "Kumamoto revised version": Futagawa-Hinagu Fault Zone and its vicinity, Geospatial Information Authority of Japan.
- Kumahara, Y., Goto, H., Nakata, T., Ishiguro, S., Ishimura, D., Ishiyama, T., Okada, S., Kagohara, K., Kashiwabara, S., Kaneda, H., Sugito, N., Suzuki, Y., Takenami, D., Tanaka, K., Tanaka, T., Tsutsumi, H., Toda, S., Hirouchi, D., Matsuta, N., Mita, T., Moriki, H., Yoshida, H. and Watanabe, M. (2016): Distribution of surface rupture associated the 2016 Kumamoto earthquake and its significance, *JpGU Meeting 2016*, May 22-26, 2016, Chiba, Japan.
- Mitsugami, I. (2011). Bundler: Structure from motion for unordered image collections, *The Journal of The Institute of Image Information and Television Engineers*, 65, 479-482, DOI: 10.3169/itej.65.479 (in Japanese)
- Nakano, T. (2017). Parameter analysis for practical application of earthquake safety evaluation of residential fill and development of generation method of topography data, *Research result report of KAKENHI*, <https://kaken.nii.ac.jp/ja/file/KAKENHI-PROJECT-15K16288/15K16288seika.pdf> (accessed 14 Nov, 2018) (in Japanese with English abstract)
- Nakano, T., Kobayashi, T., Yoshida, K. and Fujiwara S. (2016a). Field survey of non-tectonic surface displacements caused by the 2016 Kumamoto Earthquake around Aso Valley, *Bulletin of GSI of Japan*, 64, 47-54.
- Nakano, T., Wada, K., Yamanaka, M., Kamiya, I. and Nakajima, H. (2016b). Precursory slope deformation around landslide area detected by InSAR throughout Japan, *The International Archives of the Photogrammetry, Remote Sensing and Spatial Information Sciences, Volume XLI-B1*, 1201-1205, DOI:10.5194/isprsarchives-XLI-B1-1201-2016
- Suzuki, Y., Ishimura, D., Kumaki, Y., Kumahara, Y., Chida, N., Nakata, T. and Nakano, T. (2017): 1:25,000 Active Fault Map "Aso": Futagawa-Hinagu Fault Zone and its vicinity, Geospatial Information Authority of Japan.
- Tsuji, T., Ishibashi, J., Ishitsuka K. and Kamata, R. (2017). Horizontal sliding of kilometer-scale hot spring area during the 2016 Kumamoto earthquake, *Scientific Reports*, 7:42947, DOI: 10.1038/srep42947
- Une, H., Sato, H.P., Yurai, H. and Tobita, M. (2008). Analysis of surface deformation induced by the Noto Hanto and the Chuetsu-oki Earthquakes in 2007 using synthetic aperture radar interferograms, *Landslide-Journal of the Japan Landslide Society*, 45, 125-131. (in Japanese with English abstract)
- Wakamatsu, K., Senna, S. and Ozawa, K. (2017). Liquefaction and its characteristics during the 2016 Kumamoto Earthquake, *Journal of Japan Association for Earthquake Engineering*, 17(4), 81-100. (in Japanese and English abstract)
- Yoshimi, M., Shimizu, H., Iwata, T., Asano, K., Okamoto, S. and Suehiro, M. (2018). Seismic reflection surveys of the western and southern extensions (Futagawa and Hinagu active fault zone) of the 2016 Kumamoto earthquake source faults, *Abstract of the 12<sup>th</sup> UJNR*, <http://cais.gsi.go.jp/UJNR/12th/document/abst/P-13.pdf>